J. Fluid Mech. (2003), *vol.* 488, *pp.* 225–244.
DOI: 10.1017/S0022112003004853 Printed in the United Kingdom

Stability analysis of near-limit stretched premixed flames

By S. MINAEV[1,2], R. FURSENKO[2], Y. JU[1]† AND C. K. LAW[1]

[1]Department of Mechanical and Aerospace Engineering, Princeton University, NJ 08544, USA

[2]Institute of Chemical Kinetics and Combustion SB RAS, Novosibirsk, 630090, Russia

(Received 14 May 2001 and in revised form 8 February 2003)

The dynamics of radiative, near-limit, stretched premixed flames was investigated analytically and numerically, with emphasis on pulsating stability for sub-unity Lewis numbers. The analysis includes both flame stretch and order-unity heat loss, and yields a dispersion equation for the stability of radiative stretched flames subjected to symmetrical and asymmetrical perturbations. The dispersion equation reduces to that of the classical thermo-diffusional stability analysis of Sivashinsky in the limit of small heat loss, small stretch rate, and infinite flame separation distance. Results show that sub-limit flames are stable near both radiation and stretch extinction limits, and that oscillation occurs only at moderate flame stretch rates. The unstable regime and the stability diagram were obtained. Numerical simulation with detailed chemical kinetics and transport models yielded results that are in good agreement with theory. The present work also provides a satisfactory explanation of the experimental results obtained in microgravity.

1. Introduction

Understanding of the propagation and stability of near- and sub-limit premixed flames not only is important for fundamental combustion research but is also relevant to the development of new combustion technologies such as those associated with low-NO_x emission, lean burn, micro-scale combustion, and material synthesis. Recent experimental and theoretical studies on near- and sub-limit combustion using stationary counterflow flames (Maruta *et al.* 1996; Ju *et al.* 1997; Buckmaster 1997) found that sub-limit flames can be established, and that there exist multiple flame regimes (near-stagnation flame, weak flame, distant flame, and normal flame) and various extinction and jump limits due to the interaction between radiation and diffusional transport. It was also shown that the flammable regimes for these flames at general Lewis numbers can be described by the so-called G- and K-shaped extinction response curves (Ju *et al.* 1997).

It is well known that the flammable regimes of flames are affected by their stability. Theoretical (Sivashinsky 1977; Joulin & Clavin 1979) and numerical (Rogg 1982; Kailasanath, Ganguly & Patnaik 1993; He & Clavin 1993) studies of the thermal-diffusion stability of the one-dimensional propagating planar flame show that the flame becomes oscillatory when the Lewis number (Le) is larger than a critical value satisfying $\beta(Le-1) > 4(1+\sqrt{3}) \approx 10.9$, where β is the Zeldovich number. Detailed numerical simulations of one-dimensional rich hydrogen/air propagating

† Author to whom correspondence should be addressed: yju@princeton.edu

planar flames (Christiansen, Sung & Law 1998) demonstrated that the flammability limit due to radiative loss is substantially narrowed when pulsating instability is taken into account. However, all these studies were mainly concerned with pulsating instabilities of unstretched flames at *Le* larger than the critical value.

On the other hand, microgravity experiments (Maruta *et al.* 1998) showed that lean $CH_4/O_2/He/N_2$ flames with $\beta(Le-1) \ll 10.9$ actually oscillated at equivalence ratios sufficiently larger than the flammability limit. These results differ from the previous theory in two aspects: (i) oscillation does not occur at stretch rates close to the stretch and radiation limits; (ii) oscillation does not occur at equivalence ratio close to the flammability limit. However, the mechanism controlling this phenomenon was not identified in their study. A direct numerical simulation by Ju *et al.* (2000) successfully reproduced the observed oscillation and demonstrated that this oscillation is induced by thermal radiation. The results also showed that the radiation-induced oscillation can occur at Lewis number close to unity, and offered a reasonable explanation of the micro-gravity experiment and the normal-gravity experiment in which oscillations were observed for stretched cylindrical CH_4/air flames (Kitano, Kobayashi & Otsuka 1989). However, this finding cannot be explained by the classical thermal-diffusion theory. Furthermore, due to computational limitation, the stability diagram for the entire flammable regime was not obtained. Thus, a theoretical examination of the stability and the stability diagram is necessary.

The stability of stretched flames was analysed by Buckmaster (1979), Sivashinsky & Law (1982) and Kortstarts *et al.* (1997) for adiabatic flames with small stretch and slow time evolution. However, there is no theory describing the stability of radiative, near-limit stretched flames. The purpose of the present study is therefore to study the dynamics and stability of radiative, counterflow premixed flames, and to obtain a rigorous dispersion equation and diagram for the onset of pulsating oscillation for *Le* less than unity. The mathematical model for the theoretical analysis is given in the next section, which is followed by the stationary solution and the stability analysis, and finally a numerical investigation of the stability of CH_4–air mixture with detailed chemistry.

2. Mathematical model

The configuration considered in the present study is axis-symmetrical back-to-back counterflow premixed flames. In this configuration the air–fuel mixtures are issued from two opposed burners forming two planar flames near the stagnation plane. A schematic of the twin flames and the three analytical domains (1: unburned region on the right-hand side, 2: burned gas region, and 3: unburned gas region on the left-hand side) are shown in figure 1. By employing the conventional assumptions of constant density, constant thermal properties, potential flow, and localized reaction zone, the governing equations for temperature and fuel concentration are

$$\frac{\partial T}{\partial t} - ax\frac{\partial T}{\partial x} = \frac{\partial T}{\partial x} + (1-\sigma)(W_1 + W_3) - Q, \tag{1}$$

$$\frac{\partial C}{\partial t} - ax\frac{\partial C}{\partial x} = \frac{1}{Le}\frac{\partial^2 C}{\partial x^2} - (W_1 + W_3), \tag{2}$$

where

$$W_1 = \exp\left(\frac{N}{2}\left(1 - \frac{1}{T_f^+}\right)\right)\delta(x - x_f^+), \quad W_3 = \exp\left(\frac{N}{2}\left(1 - \frac{1}{T_f^-}\right)\right)\delta(x - x_f^-) \tag{3}$$

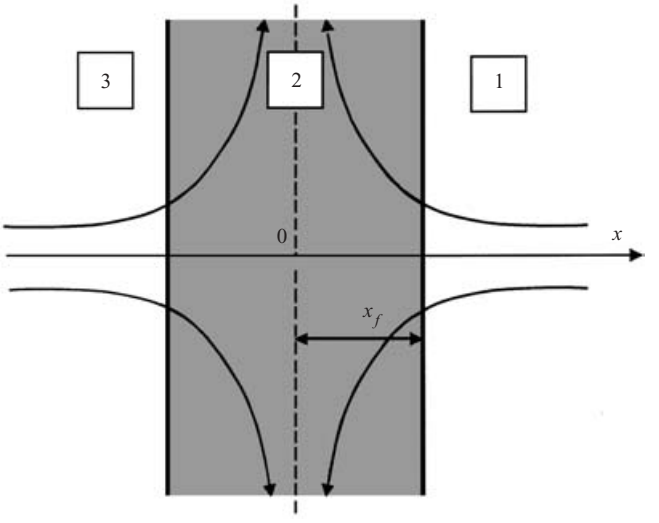

FIGURE 1. Schematic of twin flames. The dashed vertical line indicates the stagnation plane. Zones 1, 2 and 3 are three analytical regions, respectively for the unburned gas on the right-hand side, the burned gas and the unburned gas on the left-hand side.

Furthermore, t, x, C and T are the time, streamwise coordinate, temperature and fuel mass fraction, respectively normalized by D_{th}/U_{ad}^2, D_{th}/U_{ad}, T_{ad} and C_0. Here D_{th}, U_{ad}, T_{ad} and C_0 are, respectively, the thermal diffusivity, adiabatic flame speed, adiabatic flame temperature and initial mass fraction of fuel. N is the activation energy normalized by the adiabatic flame temperature, Le the Lewis number, δ the Dirac δ-function, and a the stretch rate normalized by U_{ad}^2/D_{th}. The two flame fronts are located at x_f^+ and x_f^-, respectively, on the right- and the left-hand sides of the stagnation plane ($x = 0$). For convenience of algebraic manipulation, the heat loss $Q(T)$ is approximated as a linear function of temperature. There are two possible choices for the one-parametric function $Q(T)$. In the first case, the heat loss is only considered in the burned gas region and the heat loss in the unburned gas region is ignored, i.e.

$$Q = h(T_2 - \sigma), \quad x_f^- < x < x_f^+,$$
$$Q = 0, \quad x_f^+ < x < +\infty, \ -\infty < x < x_f^-,$$

where h is the intensity of radiation heat loss normalized by U_{ad}^2/D_{th} and σ is the ratio of the initial temperature to the adiabatic flame temperature. This approximation was applied in the theoretical study of 'flame balls' (Buckmaster, Joulin & Ronney 1991). The other possible choice for Q is that the heat loss occurs in both the unburned and the burned gas regions. In this case, $Q = h(T - \sigma)$ holds everywhere. This approach was also applied in the study of counterflow flames (Buckmaster 1997). It should be noted that, in this simple model, the detailed specification of concentration of the radiating species is not included. Thus, there is arbitrariness in the choice of the one-parametric heat-loss term. In the present study, we employed both formulations of heat loss by paying more attention to the first. By introducing an integer $n = 0, 1$ the heat-loss term may be written in the form

$$\left.\begin{aligned} Q &= h(T_2-\sigma), \quad x_f^- < x < x_f, \\ Q &= nh(T_1-\sigma), \quad x_f^+ < x < +\infty, \\ Q &= nh(T_3-\sigma), \quad -\infty < x < x_f^-. \end{aligned}\right\} \tag{4}$$

The case of $n=0$ corresponds to the first choice of Q in which heat loss in the unburned region is ignored. The case of $n=1$ includes heat loss everywhere.

By employing the new time and spatial variables $\tau = at/2$, $\varsigma = x\sqrt{a/2}$ and $H = h/a$, the governing equations (1)–(4) may be written as

$$\frac{\partial T_1}{\partial \tau} - 2\varsigma\frac{\partial T_1}{\partial \varsigma} = \frac{\partial^2 T_1}{\partial \varsigma^2} - 2nH(T_1-\sigma) \quad \text{for} \quad \varsigma_f^+ < \varsigma < +\infty, \tag{5}$$

$$\frac{\partial C_1}{\partial \tau} - 2\varsigma\frac{\partial C_1}{\partial \varsigma} = \frac{1}{Le}\frac{\partial^2 C_1}{\partial \varsigma^2} \quad \text{for} \quad \varsigma_f^+ < \varsigma < +\infty, \tag{6}$$

$$\frac{\partial T_2}{\partial \tau} - 2\varsigma\frac{\partial T_2}{\partial \varsigma} = \frac{\partial^2 T_2}{\partial \varsigma^2} - 2H(T_2-\sigma) \quad \text{for} \quad \varsigma_f^- < \varsigma < \varsigma_f^+, \tag{7}$$

$$\frac{\partial T_3}{\partial \tau} - 2\varsigma\frac{\partial T_3}{\partial \varsigma} = \frac{\partial^2 T_3}{\partial \varsigma^2} - 2nH(T_3-\sigma) \quad \text{for} \quad -\infty < \varsigma < \varsigma_f^-, \tag{8}$$

$$\frac{\partial C_3}{\partial \tau} - 2\varsigma\frac{\partial C_3}{\partial \varsigma} = \frac{1}{Le}\frac{\partial^2 C_3}{\partial \varsigma^2} \quad \text{for} \quad -\infty < \varsigma < \varsigma_f^-. \tag{9}$$

In the above, the subscripts 1, 2 and 3 respectively correspond to the regions of the fresh mixture in the right-half ($\varsigma_f^+ < \varsigma < +\infty$), the combustion products ($\varsigma_f^- < \varsigma < \varsigma_f^+$), and the fresh mixture in the left-half ($-\infty < \varsigma < \varsigma_f^-$) (see figure 1). Since fuel is completely consumed in the burned gas region, the boundary conditions for equations (5)–(9) can be given as

$$T_1 \to \sigma, \quad C_1 \to 1 \quad \text{as} \quad \varsigma \to +\infty, \quad T_3 \to \sigma, \quad C_3 \to 1 \quad \text{as} \quad \varsigma \to -\infty, \tag{10}$$

$$\frac{\partial T_2(-0)}{\partial \varsigma} = \frac{\partial T_2(+0)}{\partial \varsigma}0, \quad T_2(-0) = T_3(+0) \quad \text{as} \quad \varsigma = 0, \tag{11}$$

and the jump conditions at the flame interfaces ($\varsigma = \varsigma_f^{\pm}$) are

$$\frac{\partial T_2}{\partial \varsigma} - \frac{\partial T_1}{\partial \varsigma} = \frac{(1-\sigma)}{Le}\frac{\partial C_1}{\partial \varsigma}, \tag{12}$$

$$\frac{1}{Le}\sqrt{\frac{a}{2}}\frac{\partial C_1}{\partial \varsigma} = \exp\left(\frac{N}{2}\left(1-\frac{1}{T_f^+}\right)\right), \tag{13}$$

$$T_1 = T_2 = T_f^+, \tag{14}$$

$$C_1 = 0, \tag{15}$$

$$\frac{\partial T_2}{\partial \varsigma} - \frac{\partial T_3}{\partial \varsigma} = \frac{(1-\sigma)}{Le}\frac{\partial C_3}{\partial \varsigma}, \tag{16}$$

$$-\frac{1}{Le}\sqrt{\frac{a}{2}}\frac{\partial C_3}{\partial \varsigma} = \exp\left(\frac{N}{2}\left(1-\frac{1}{T_f^-}\right)\right), \tag{17}$$

$$T_3 = T_2 = T_f^-, \tag{18}$$

$$C_3 = 0. \tag{19}$$

Equations (12)–(15) and (16)–(19) are the boundary conditions at the flame interfaces of $\varsigma = \varsigma_f^+$ and $\varsigma = \varsigma_f^-$, respectively.

Following Buckmaster (1997), we assume that thermal radiation is due to the emission of the burned gas products such as H_2O and CO_2, so that the magnitude of dimensional radiation loss $hU_{ad}^2(\sigma)/D_{th}$ is proportional to the mass fraction of the deficient reactant C_0. If h_c at a given value of σ_c is known, the value h at any σ can be found through

$$h(\sigma) = h_c \frac{C_0(\sigma)}{C_0(\sigma_c)} \frac{U_{ad}^2(\sigma_c)}{U_{ad}^2(\sigma)}, \tag{20}$$

where

$$C_0(\sigma) = \frac{C_p T_0}{q}\left(\frac{1}{\sigma} - 1\right), \quad \frac{U_{ad}^2(\sigma_c)}{U_{ad}^2(\sigma)} = \exp\left(\frac{T_a}{T_0}(\sigma - \sigma_c)\right). \tag{21}$$

By applying this model to the planar propagating flame subjected to radiative heat loss, we obtain the classical formula for the critical heat losses at the flammability limit (Buckmaster & Ludford, 1983):

$$h_c = \frac{1}{(n+1)e} \frac{T_c^2}{T_a(T_c - T_0)} = \frac{T_0}{(n+1)eT_a} \frac{1}{\sigma_c(1-\sigma_c)}. \tag{22}$$

The above formula allows us to specify the critical value of the radiative heat loss parameter h_c via the critical flame temperature at the flammability limit for a given mixture. Here, we have used the data recommended by Buckmaster (1997), and have chosen $T_0 = 300\,\mathrm{K}$, $T_a = 15000\,\mathrm{K}$, $Le = 0.9$, which correspond roughly to a lean methane–air mixture. The resulting dimensional flame temperature at lean flammability limit is $T_c = 1300\,\mathrm{K}$ and $\sigma_c = T_0/T_c \approx 0.23$.

3. Stationary solutions

For a stationary analysis, it is reasonable to limit our attention to the symmetrical solution. In this case, instead of using the boundary conditions (11), we can apply the symmetry condition at $\varsigma = 0$:

$$\frac{\partial T_2}{\partial \varsigma} = 0. \tag{23}$$

The problem defined by equations (5)–(7) and the boundary conditions (10), (12)–(15) and (23) has the following solution:

$$T_{1s} = \sigma + (T_{fs}^+ - \sigma)\frac{I^-(\varsigma, nH)}{I^-(\varsigma_{fs}^+, nH)}, \tag{24}$$

$$T_{2s} = \sigma + (T_{fs}^+ - \sigma)\frac{I^+(\varsigma, H) + I^-(\varsigma, H)}{I^+(\varsigma_{fs}^+, H) + I^-(\varsigma_{fs}^+, H)}, \tag{25}$$

$$C_{1s} = \frac{\mathrm{erf}(\sqrt{Le}\varsigma) - \mathrm{erf}(\sqrt{Le}\varsigma_{fs}^+)}{1 - \mathrm{erf}(\sqrt{Le}\varsigma_{fs}^+)}, \tag{26}$$

where

$$\mathrm{erf}(\varsigma) = \frac{2}{\sqrt{\pi}} \int_0^{\varsigma} \exp(-\eta^2)\,\mathrm{d}\eta$$

and

$$I^{-}(\varsigma, \Lambda) = \exp(-\varsigma^2) \int_0^{\infty} \eta^{\Lambda} \exp\left(-\frac{\eta^2}{4} - \varsigma\eta\right) \mathrm{d}\eta, \tag{27}$$

$$I^{+}(\varsigma, \Lambda) = \exp(-\varsigma^2) \int_0^{\infty} \eta^{\Lambda} \exp\left(-\frac{\eta^2}{4} + \varsigma\eta\right) \mathrm{d}\eta. \tag{28}$$

The solution of equation (26) for C_{1s} is straightforward. It is noted that, for the first time, exact solutions for equations (5) and (7) with boundary conditions (10), (14) and (23) have been found. Proofs of these solutions are given in the Appendix. The temperature and concentration distributions in the half-plane $\varsigma < 0$ can be found from (24)–(26) using the substitutions

$$T_3(\varsigma) = T_2(-\varsigma), \quad C_3(\varsigma) = C_1(-\varsigma), \quad \varsigma_{fs}^{+} = -\varsigma_{fs}^{-}, \quad T_{fs}^{+} = T_{fs}^{-}.$$

It is noted that exact solutions (24)–(26) remove the requirement of the small-heat-loss assumption ($hx_{fs} \approx 1/N \ll 1$), which is a common asymptotic approach in previous studies but obviously becomes incorrect as $x_{fs} \to \infty$. Therefore our method provides a direct way to understand the relation between the stretched stagnation flame and the far-field planar propagating flame in the small-stretch limit.

By substituting equations (24)–(26) into (12)–(13), one obtains an algebraic system of equations for the flame separation distance $x_{fs} = \varsigma_{fs}^{+}\sqrt{2/a}$ and the flame temperature T_{fs},

$$\sqrt{\frac{a}{2Le}}\,\psi(\sqrt{Le}\,\varsigma_{fs}^{+}) = \exp\left(\frac{N}{2}\left(1 - \frac{1}{T_{fs}}\right)\right), \tag{29}$$

$$(T_{fs} - \sigma)(B_S(\varsigma_{fs}^{+}, H) - A(\varsigma_{fs}^{+}, nH)) = \frac{(1-\sigma)}{\sqrt{Le}}\psi(\sqrt{Le}\,\varsigma_{fs}^{+}), \tag{30}$$

where

$$\psi(\varsigma) = \frac{2}{\sqrt{\pi}}\frac{\exp(-\varsigma^2)}{1 - \mathrm{erf}(\varsigma)}, \tag{31}$$

$$A(\varsigma, \Lambda) = \frac{\mathrm{d}}{\mathrm{d}\varsigma}\ln(I^{-}(\varsigma, \Lambda)), \tag{32}$$

$$B_S(\varsigma, \Lambda) = \frac{\mathrm{d}}{\mathrm{d}\varsigma}\ln(I^{+}(\varsigma, \Lambda) + I^{-}(\varsigma, \Lambda)). \tag{33}$$

In the limit of $x_{fs} \to 0$ and $\varsigma_{fs}^{+} \to 0$, (29) and (30) yield the flame stretch a_{ext} and flame temperature at the stretch extinction limit T^{*},

$$a_{ext} = \frac{\pi Le}{2}\exp\left(\frac{N(T^{*} - 1)}{T^{*}}\right), \quad T^{*} = \sigma + \frac{1-\sigma}{\sqrt{Le}}. \tag{34}$$

It is seen from (34) that the Lewis number has a strong effect on the stretch extinction. A decrease of Le results in an increase of the extinction temperature and the stretch limit. In the limiting case of $a \to 0$, $\varsigma_{fs}^{+} \to \infty$, $H = h/a \to \infty$, the function $\psi(\sqrt{Le}\,\varsigma_{fs}^{+})$ defined by (31) may be written in the form

$$\psi(\sqrt{Le}\varsigma_{fs}^{+}) \approx 2\sqrt{Le}\,\varsigma_{fs}^{+} + O\left(\frac{1}{\varsigma_{fs}^{+}}\right)^2. \tag{35}$$

In view of (35), equation (29) readily becomes

$$T_{fs} = 1 \Big/ \left(1 - \frac{2}{N} \ln V_f\right), \tag{36}$$

where $V_f = \sqrt{2a}\varsigma_{fs}^+ = ax_f$ is the gas velocity entering the flame front. In the limit of infinite flame separation distance, $\varsigma_{fs}^+ \to \infty$, the integral $I^-(\varsigma_{fs}^+)$ in (28) vanishes so that (30) is reduced to

$$(T_{fs} - \sigma)\frac{\mathrm{d}}{\mathrm{d}\varsigma_{fs}^+}(\ln I^+(\varsigma_{fs}^+, H) - \ln I^-(\varsigma_{fs}^+, nH)) = 2(1-\sigma)\varsigma_{fs}^+. \tag{37}$$

At large ς_{fs}^+ and H, the derivatives on the right-hand side of (37) have the forms (see Appendix)

$$\frac{\mathrm{d}}{\mathrm{d}\varsigma} \ln I^+(\varsigma, H) \approx \sqrt{\varsigma^2 + 2H} - \varsigma, \tag{38}$$

$$\frac{\mathrm{d}}{\mathrm{d}\varsigma} \ln I^-(\varsigma, nH) \approx -\sqrt{\varsigma^2 + 2nH} - \varsigma. \tag{39}$$

In the case of heat loss everywhere ($n = 1$), by using (38) and (39), equation (37) can be transformed to

$$(T_{fs} - \sigma)\sqrt{V_f^2 + 4h} = (1-\sigma)V_f. \tag{40}$$

Equations (36) and (40) are the classical formulas describing an unstrained non-adiabatic flame with flame velocity $V_f = \sqrt{2a}\varsigma_{fs}^+ = ax_{fs}$. For $h < h_c$, there are two solutions (a stable solution with large velocity $\mathrm{e}^{-1/2} < V_f < 1$ and an unstable solution with small velocity $0 < V_f < \mathrm{e}^{-1/2}$). At $h = h_c$, the two solutions merge at $V_f = \mathrm{e}^{-1/2}$, which is the flammability limit.

By calculating (29) and (30) for $Le = 0.9$, the typical relation between flame separation distance and stretch rate for the sub-limit ($\sigma = 0.23$, $n = 0$) and near-limit ($\sigma = 0.22$, $n = 0, 1$) stretch flames are shown in figures 2 and 3. It is seen that the present result qualitatively reproduces previous findings (Ju *et al.* 1997 and Buckmaster 1997). A detailed description and classification of the separate branches of these curves in figuers 2 and 3 are given by Ju *et al.* (1997, 1998). Here, for brevity, we only give a brief summary of the bifurcations. In sub-limit flame bifurcations (figure 2), branch (*a*) is the distant flame (DF), (*b*) the unstable slow burning flow, and (*c*) the near-stagnation flame (NSF). For the near-limit flame (equivalence ratio slightly higher than the fundamental limit of a one-dimensional planar propagating flame), the DF and NSF branches in figure 2 merge, resulting in a new bifurcation pattern (figure 3) in which branch (*e*) is the normal flame (this is the flame extensively investigated in normal gravity (Law 1988), and (*d*) is the weak flame branch (WF). In figure 3, the dependence of $x_f(a)$ on the stretch rate is plotted for both the one-sided ($n = 0$) and two-sided ($n = 1$) heat-loss approximations. Both approximations yield quite similar solution curves associated with the normal flame (*e*) and the slow burning flow (*b*). The difference between the results of these two formulations arises at small stretch rates and flame location distances. Unlike the results of a model with from both sides heat losses and results of previous studies (Ju *et al.* 1997, 1998), where weak flame quenching takes place at small strain rates, this radiation-dominated quenching limit is lacking in the case of one-sided heat loss formulation because the heat loss in the unburned region is ignored. The dependence of flame temperature on strain rate corresponding to figures 2 and 3 is shown in figures 4 and 5, respectively.

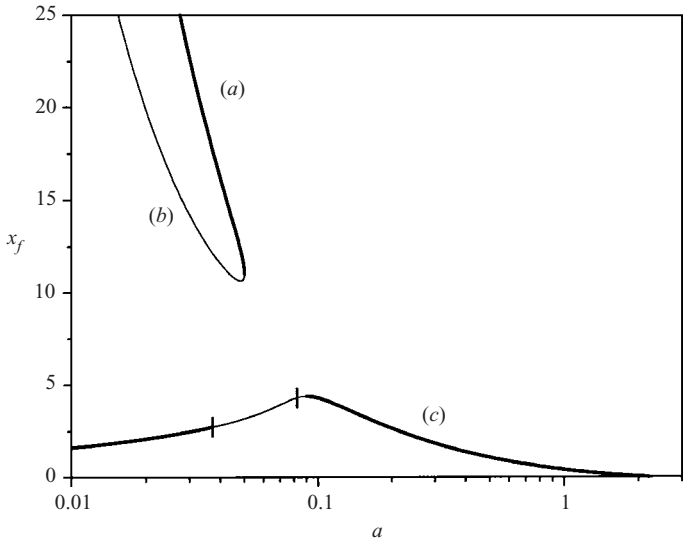

FIGURE 2. Flame separation distance x_f vs. non-dimensional stretch rate a for $Le = 0.9$, $\sigma = 0.23$ and $n = 0$. The thick lines denote the stable regions of the distant flame branch (a) and the near-stagnation flame branch (c). The thin line on branch (b) represents the unstable slow burning flow, and the thin line on branch (c) denotes the region of pulsating instability of the near-stagnation flame.

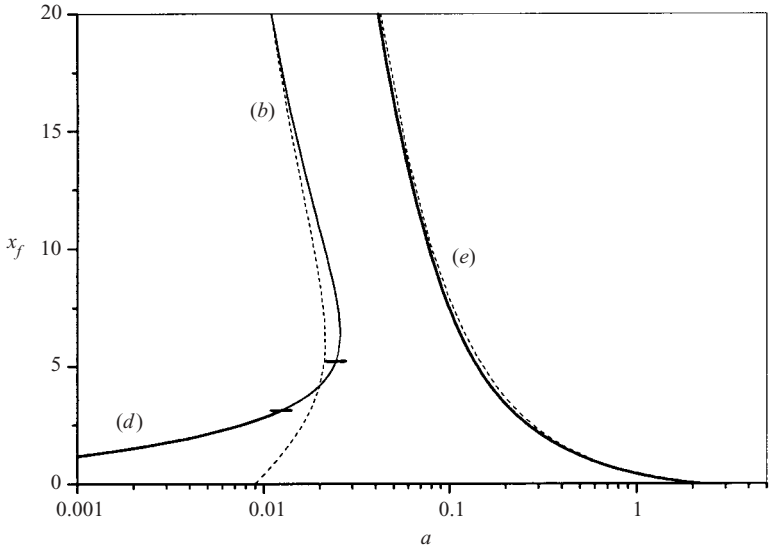

FIGURE 3. Flame separation distance x_f vs. non-dimensional stretch rate a for $Le = 0.9$ and $\sigma = 0.22$ for $n = 0$ (solid lines) and $n = 1$ (dashed lines). The thick solid lines denote the stable normal flame (e) and weak flame (d) branches. Thin solid line of branch (b) indicates the unstable region of the slow burning flame. The thin line on the right part of (d) branch represents the pulsating region of the weak flame.

4. Linear stability analysis

The stability of the complex bifurcations was not discussed in previous studies (Ju *et al.* 1997; Buckmaster 1997; Ju *et al.* 1999), although clarification of the

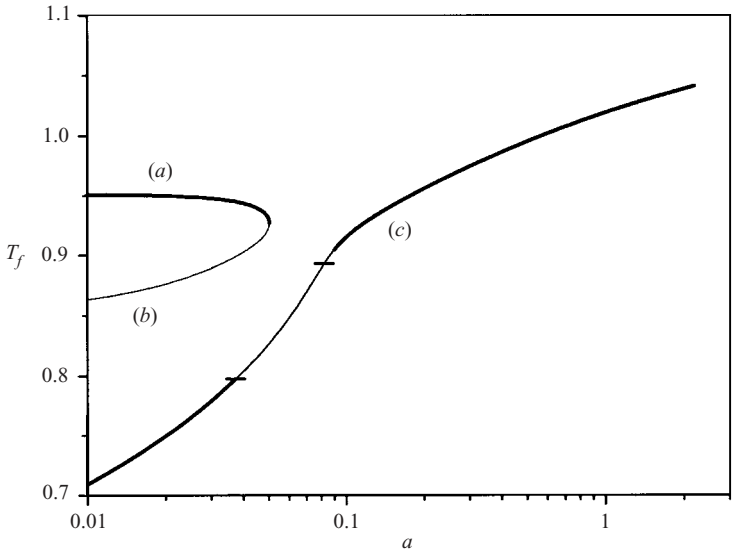

FIGURE 4. Flame temperature T_f vs. stretch rate a for $Le = 0.9$, $\sigma = 0.23$ and $n = 0$. Notation of the solution curves is the same as in figure 2.

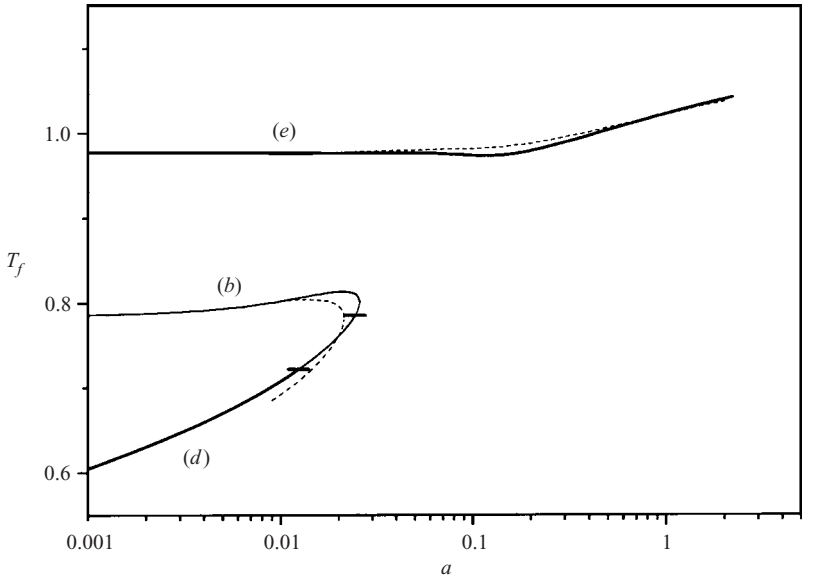

FIGURE 5. Flame temperature T_f vs. stretch rate a for $Le = 0.9$, $\sigma = 0.22$ and $n = 0, 1$. Notation of the solution curves is the same as in figure 3.

stability of the sub-limit flame is of great importance. The main goal of the present study is the linear stability analysis of the sub-limit flames, including the case of asymmetrical perturbations.

The linear stability of the stationary solution of the previous section can be determined by examining the growth rate of infinitesimal perturbations of variable $\tilde{\phi}$:

$$\left.\begin{aligned} &T_1 = T_{1s} + \tilde{T}_1\tilde{\phi}, \quad T_2 = T_{2s} + \tilde{T}_2\tilde{\phi}, \quad T_3 = T_{3s} + \tilde{T}_3\tilde{\phi}, \quad C_1 = C_{1s} + \tilde{C}_1\tilde{\phi}, \\ &C_3 = C_{3s} + \tilde{C}_3\tilde{\phi}, \quad T_f^{\pm} = T_{fs} + \tilde{T}_{fs}^{\pm}\tilde{\phi}, \quad \varsigma_{fs}^{\pm} = \pm\varsigma_{fs}^{+} + \tilde{\varsigma}_f^{\pm}\tilde{\phi}, \end{aligned}\right\} \tag{41}$$

where $\tilde{\phi}$ is assumed to be proportional to $\exp(2\Omega\tau)$. By substituting the above expansions into (5)–(9), the solutions of the perturbations as functions of ς and Ω are given by

$$\left.\begin{aligned} &\tilde{T}_1 = a_1 I^-(\varsigma, \Omega + nH), \quad \tilde{T}_2 = a_2 I^+(\varsigma, \Omega + H) + a_3 I^-(\varsigma, \Omega + H), \\ &\tilde{T}_3 = a_4 I^+(\varsigma, \Omega + nH), \quad \tilde{C}_1 = a_5 I^-(\varsigma\sqrt{Le}, \Omega), \quad \tilde{C}_3 = a_6 I^+(\varsigma\sqrt{Le}, \Omega), \end{aligned}\right\} \tag{42}$$

where a_i are the constants and the functions I^-, I^+ are defined by (27) and (28).

As shown in the Appendix, $I^-(\varsigma, \Omega)$ and $I^+(\varsigma, \Omega)$ are the exact solutions of the equation

$$\frac{\mathrm{d}^2\phi}{\mathrm{d}\varsigma^2} + 2\varsigma\frac{\mathrm{d}\phi}{\mathrm{d}\varsigma} - 2\Omega\phi = 0, \tag{43}$$

and $I^-(\varsigma) \to 0$ as $\varsigma \to \infty$ whereas $I^+(\varsigma)$ diverges at infinitely large ς. By taking into account that $T_1'(\varsigma) \to 0$ and $C_1'(\varsigma) \to 0$ as $\varsigma \to \infty$, the solutions for T_1' and C_1' are chosen to be proportional to $I^-(\varsigma)$.

By then substituting (42) into the boundary conditions (12)–(19), and expanding it near the flame location, the linearized boundary conditions (12)–(19) at the flame front may be written as

$\varsigma = \varsigma_{fs}^{+}$:

$$\frac{\mathrm{d}\tilde{T}_2}{\mathrm{d}\varsigma} - \frac{\mathrm{d}\tilde{T}_1}{\mathrm{d}\varsigma} - \frac{1-\sigma}{Le}\frac{\mathrm{d}\tilde{C}_1}{\mathrm{d}\varsigma} + \left(\frac{\mathrm{d}^2T_{2s}}{\mathrm{d}\varsigma^2} - \frac{\mathrm{d}^2T_{1s}}{\mathrm{d}\varsigma^2} - \frac{1-\sigma}{Le}\frac{\mathrm{d}^2C_{1s}}{\mathrm{d}\varsigma^2}\right)\tilde{\varsigma}_f^{+} = 0, \tag{44}$$

$$\frac{\mathrm{d}^2C_{1s}}{\mathrm{d}\varsigma^2}\tilde{\varsigma}_f^{+} + \frac{\mathrm{d}\tilde{C}_1}{\mathrm{d}\varsigma} = \frac{N}{2T_{fs}^2}\frac{\mathrm{d}C_{1s}}{\mathrm{d}\varsigma}\tilde{T}_f^{+}, \tag{45}$$

$$\frac{\mathrm{d}T_{1s}}{\mathrm{d}\varsigma}\tilde{\varsigma}_f^{+} + \tilde{T}_1 = \frac{\mathrm{d}T_{2s}}{\mathrm{d}\varsigma}\tilde{\varsigma}_f^{+} + \tilde{T}_2 = \tilde{T}_f^{+}, \tag{46}$$

$$\frac{\mathrm{d}C_{1s}}{\mathrm{d}\varsigma}\tilde{\varsigma}_f^{+} + \tilde{C}_1 = 0; \tag{47}$$

$\varsigma = -\varsigma_{fs}^{+}$:

$$\frac{\mathrm{d}\tilde{T}_3}{\mathrm{d}\varsigma} - \frac{\mathrm{d}\tilde{T}_2}{\mathrm{d}\varsigma} + \frac{1-\sigma}{Le}\frac{\mathrm{d}\tilde{C}_3}{\mathrm{d}\varsigma} + \left(\frac{\mathrm{d}^2T_{3s}}{\mathrm{d}\varsigma^2} - \frac{\mathrm{d}^2T_{2s}}{\mathrm{d}\varsigma^2} + \frac{1-\sigma}{Le}\frac{\mathrm{d}^2C_{3s}}{\mathrm{d}\varsigma^2}\right)\tilde{\varsigma}_f^{-} = 0, \tag{48}$$

$$\frac{\mathrm{d}^2C_{3s}}{\mathrm{d}\varsigma^2}\tilde{\varsigma}_f^{-} + \frac{\mathrm{d}\tilde{C}_3}{\mathrm{d}\varsigma} = \frac{N}{2T_{fs}^2}\frac{\mathrm{d}C_{3s}}{\mathrm{d}\varsigma}\tilde{T}_f^{-}, \tag{49}$$

$$\frac{\mathrm{d}T_{3s}}{\mathrm{d}\varsigma}\tilde{\varsigma}_f^{-} + \tilde{T}_3 = \frac{\mathrm{d}T_{2s}}{\mathrm{d}\varsigma}\tilde{\varsigma}_f^{-} + \tilde{T}_2 = \tilde{T}_f^{-}, \tag{50}$$

$$\frac{\mathrm{d}C_{3s}}{\mathrm{d}\varsigma}\tilde{\varsigma}_f^{-} + \tilde{C}_3 = 0. \tag{51}$$

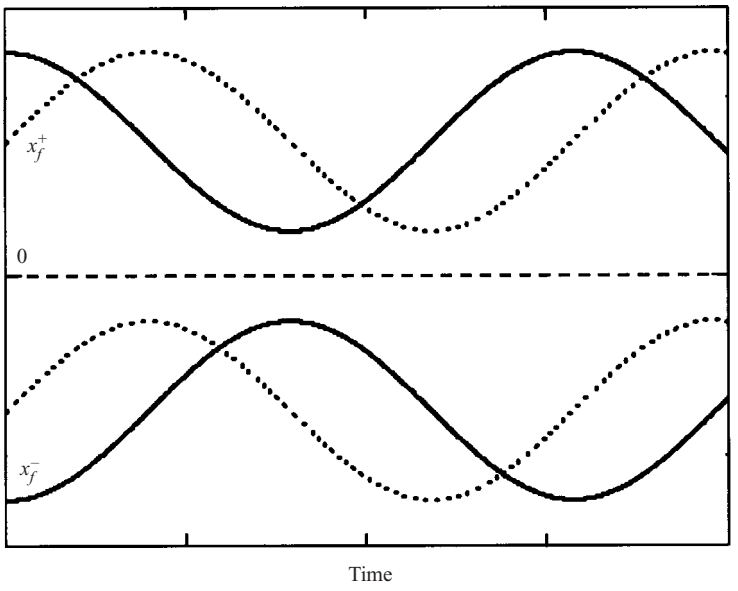

FIGURE 6. Oscillatory evolution history of the flame front location (x_f^+, x_f^-). Solid lines denote the symmetric oscillations and the dashed lines denote the asymmetric oscillations.

The above equations yields the dispersion relation for Ω of the form

$$D_S D_A = 0, \tag{52}$$

where

$$\begin{aligned} D_{S,A} = {} & 2H(T_{fs} - \sigma) + \frac{1-\sigma}{\sqrt{Le}}\psi(\varsigma_{fs}^+\sqrt{Le})(A(\varsigma_{fs}^+\sqrt{Le}, \Omega) - B_{S,A}(\varsigma_{fs}^+, \Omega + H) \\ & + 2\varsigma_{fs}^+(Le-1)) + (A(\varsigma_{fs}^+, \Omega + nH) - B_{S,A}(\varsigma_{fs}^+, \Omega + H)) \\ & \times \left(\frac{2T_{fs}^2}{N}(2\varsigma_{fs}^+ Le + A(\varsigma_{fs}^+\sqrt{Le}, \Omega)) + (T_{fs}^+ - \sigma)A(\varsigma_{fs}^+, nH)\right). \end{aligned} \tag{53}$$

Here ψ is defined by (31), and A and B_S are defined by (32) and (33), respectively. In addition,

$$B_A(\varsigma, \Lambda) = \frac{\mathrm{d}}{\mathrm{d}\varsigma}\ln(I^+(\varsigma, \Lambda) - I^-(\varsigma, \Lambda)). \tag{54}$$

As one can see from (52) that its solution consists of solutions of $D_S = 0$ and $D_A = 0$, which can be found independently. The first dispersion equation $D_S = 0$ corresponds to the case of symmetrical perturbations ($\tilde{\varsigma}_f^- = -\tilde{\varsigma}_f^+$) and the second case, $D_A = 0$, may be associated with asymmetrical or anti-symmetrical perturbations ($\tilde{\varsigma}_f^+ \neq \tilde{\varsigma}_f^-$). In the case of asymmetrical perturbations the flame separation distance remains invariable. The equality of the distance between the flames and the plane $\varsigma = 0$ characterizes the case of symmetrical perturbations. The ς_f^+, ς_f^- dependence on time in the case of symmetrical and anti-symmetrical flame oscillations is shown qualitatively in figure 6.

At large flame separation distances ($\varsigma_{fs} \to \infty$) and small velocity gradients ($a \to 0$) such that the flame velocity $V_f = x_{fs}a = \sqrt{2a}\varsigma_{fs}$ remains finite, the dispersion relation

may be transformed to (see Appendix for details)

$$\sqrt{V_f^2+4(h+\omega)}\left((T_{fs}-\sigma)\left(V_f+\sqrt{V_f^2+4h}\right)+\frac{2T_f^2Le}{N}\left(\sqrt{V_f^2+4\omega/Le}-V_f\right)\right)$$
$$=(1-\sigma)V_f\left(V_f(1-Le)+\sqrt{(LeV_f)^2+4Le\omega}+\sqrt{V_f^2+4(h+\omega)}\right) \quad (55)$$

where $\omega=\Omega a$ is the growth rate of small perturbations in the unit of U_{ad}^2/D_{th}.

In the limit of small heat loss ($h=0$, $V_f=1$, $T_f=1$) and near-unity Lewis number ($Le\to 1, N\to\infty, \beta(Le-1)=(1-\sigma)(Le-1)N$ is a finite quantity), (55) can be rewritten as

$$(2+8\omega+\beta(Le-1))(\sqrt{1+4\omega}-1)-4\beta(Le-1)\omega=0, \quad (56)$$

which is identical to that given by the theory of thermal-diffusion stability of the planar adiabatic flame (Sivashinsky 1977). According to this theory the flame becomes oscillatory when $\beta(Le-1)>4(\sqrt{3}+1)$, which follows from (56). Thus, the dispersion equation (52) for stretched flames becomes the classical dispersion relation for the freely propagating flame in the limits of small stretch rates and large flame separation distances.

The equations $D_S=0$ and $D_A=0$ were solved numerically to identify unstable stationary solutions. A stationary solution is considered to be unstable if any root of the dispersion equation (52) has positive real parts ($\mathrm{Re}(\Omega)\geqslant 0$). Numerical calculations of the growth rates Ω for different branches of $x_f(a)$ curves in figures 2 and 3 are conducted. To render experimental comparison possible, we rewrite the growth rate in the form of

$$\Omega=(\gamma+\mathrm{i}\omega)/a, \quad (57)$$

in which ω is the oscillation angular frequency normalized by U_{ad}^2/D_{th}. For the sub-limit flame regime (figures 2 and 4), calculations of (52) for the case of $n=0$ shows that on the DF branch ((*a*) in figure 2), all the roots of (52) have negative real parts and the imaginary parts are absent. Thus the DF branch is stable.

On the other hand, the calculated growth rate related to the slow-burning flame regime ((*b*) in figure 2) has a positive real part which vanishes at the neutral stability point. Thus, the slow-burning branch is unstable. This result agrees with previous inference (Ju *et al.* 1997, 1999) and numerical prediction (Ju *et al.* 2000). In fact, the DF and the slow-burning flame respectively reduce to the fast- and slow-burning regimes of the planar propagating flames in the limit of zero stretch rates. It is well known that for the planar propagating flame, the fast mode is stable and the slow mode is unstable. Therefore, the present result is consistent with the previous finding in the limit of zero stretch rates. On the NSF branch ((*c*) in figure 2), the non-dimensional real and imaginary parts of the growth rates are plotted as functions of the stretch rate in figure 7(*a*). The calculation shows that the growth rate of symmetric perturbations has positive real and non-zero imaginary parts within some range of moderate stretch rates. The imaginary part of the growth rate of anti-symmetrical perturbations is zero. The lower boundary of instability is defined by symmetrical perturbations whereas the upper boundary is defined by anti-symmetrical perturbations that dominate at stretch rates close to the upper boundary of instability. It is seen that the real part of the growth rate becomes positive only at moderate stretch rates and that there are no solutions with positive real part at small and large stretch rates. Therefore, the NSF is stable at both small and large stretch rates, and only becomes pulsating at moderate stretch rates.

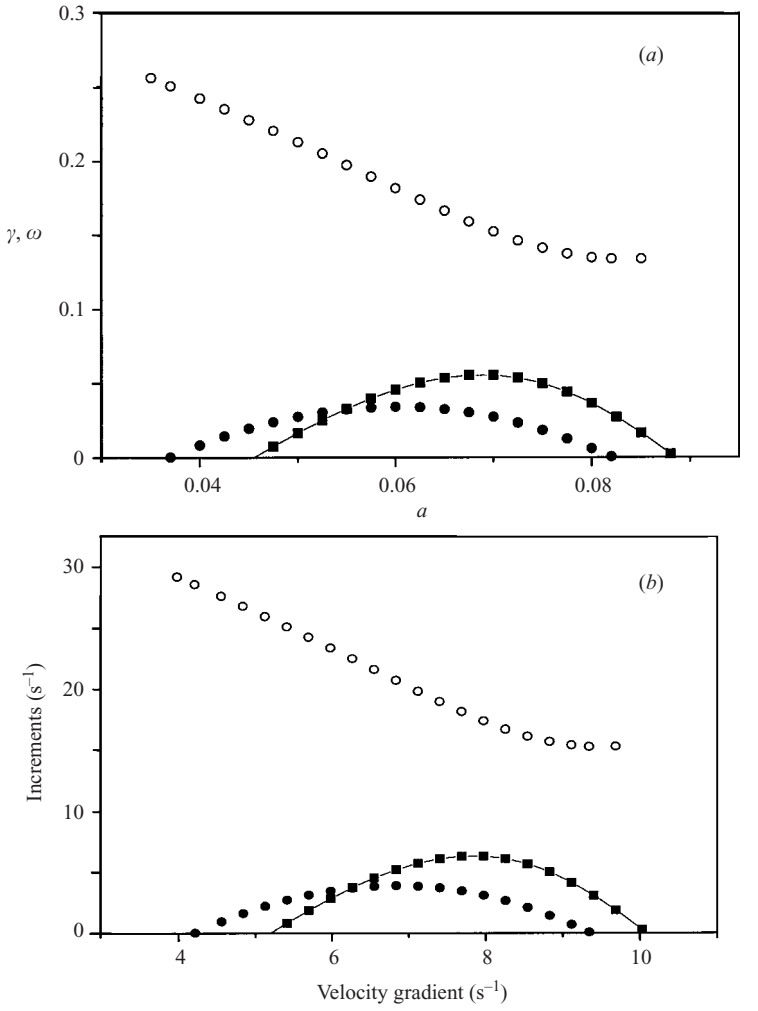

FIGURE 7. (*a*) Non-dimensional imaginary ω (open circles) and real γ (filled circles and filled squares) parts of growth rates vs. velocity gradient a for $Le = 0.9$, $\sigma = 0.23$, $n = 0$. The curve marked by squares refers to the asymmetric instability. (*b*) The dimensional growth rate vs. dimensional velocity gradient corresponding to (*c*).

The above results agree with the numerical prediction of Ju *et al.* (2000), in which it is found that the flame is stable near both the radiation extinction limit (small stretch rate) and the stretch extinction limit, and is unstable only at moderate stretch rates. Again, the present analysis shows that the mechanism of oscillations in sub- and near-limit stretched flames is different from the instability analysed by Sivashinsky (1977) and Joulin & Clavin (1979), in which pulsating instability is predicted for either very large Lewis numbers or close to the extinction limit. The dimensional growth rate corresponding to figure 7(*a*) is given in figure 7(*b*). It is seen that the oscillation frequency ($\omega/2\pi$) is between 2.5 and 4.5 Hz. By recalling that the frequency predicted in a detailed numerical simulation (Ju *et al.* 2000) is between 2 and 3 Hz and the observed frequency in microgravity experiments (Maruta *et al.* 1998) is 1.5 Hz, it can be concluded that the present analysis yields the correct description of the pulsating instability of sub-limit flames.

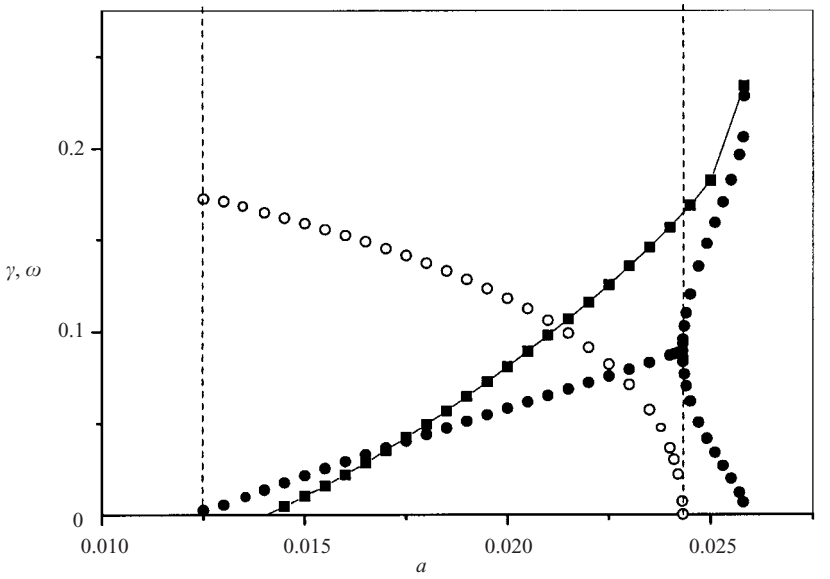

FIGURE 8. Imaginary part ω (open circles) and real part γ (filled circles and filled squares) of the growth rate vs. velocity gradient a for $Le = 0.9$, $\sigma = 0.22$, $n = 0$. The curve with squares refers to the asymmetric instability. The vertical dashed lines denote the boundaries of the pulsating instability.

For the near-limit flame regime (figure 3), calculations performed for both $n = 0$ and 1 show that the growth rates for symmetric and asymmetric perturbations are negative on the normal flame branch (e) and there are positive roots of (52) on the slow burning branch (b). This result is consistent with previous theoretical predictions (Joulin & Clavin 1979; Sivashinsky & Law 1982). However, oscillatory instability is found on the weak flame branch (d) close to its jump limit. Figure 8 shows, for the weak flame with $n = 0$, the dependence of the real and imaginary parts of the growth rate on the stretch rate in the vicinity of the turning point. The non-uniqueness of unstable solutions of the dispersion equation (52) leads to the possibility of simultaneous excitation of anti-symmetrical and symmetrical perturbations. During the development of such an instability, the pulsating flame fronts will be shifted from their symmetrical locations to either side of the stagnation plane. One of the possible scenarios of the flame behaviour in the case of excitation with both non-symmetrical and symmetrical perturbations is shown in figure 9, in which the flame front trajectory in the phase plane $(\mathrm{d}x_f/\mathrm{d}t,\ x_f)$ is plotted. This trajectory resembles to that given in Maruta *et al.* (1998). This example is presented only as illustration of the complicated flame behaviour associated with the development of this kind of instability because nonlinear analysis is need to describe the evolution of finite-amplitude perturbations.

With the further reduction of the stretch rate, the real part of the growth rate becomes negative, indicating that the weak flame is stable at small stretch rates. Therefore, on the weak flame branch, the pulsating instability only occurs in a regime near the jump limit, which corresponds to the interval between the two dashed lines in figure 8. This prediction agrees well with the direct numerical solution (Ju *et al.* 2000).

By plotting the upper and lower boundaries (stretch rate) of the pulsating instability in figures 7 and 8 as functions of the reduced adiabatic flame temperature or fuel

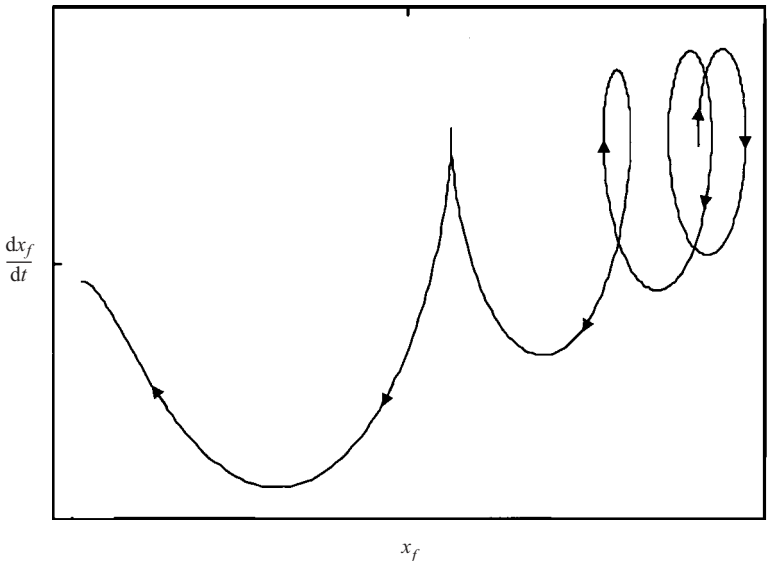

FIGURE 9. Trajectory of the flame front in the phase diagram of flame propagation velocity and flame location for the combined asymmetric and symmetric flame front perturbations: $x_f(t) = -0.14\exp(0.1t + i5.3t) - 0.1\exp(0.7t)$.

concentration $1/(\sigma - 1)$, the pulsating zone in the plane of stretch rate versus reduced flame temperature is shown in figure 10. It is seen that pulsating instability only occurs within the closed curve. This result supports the results from the direction numerical simulation, where a close unstable region was not obtained.

The current study is concerned with a stability analysis of one-dimensional perturbations. The development of unsteady two-dimensional perturbations may lead to the formation of complex non-planar and time-dependent modes of the flame front. Recent experiments (Kaiser, Liu & Ronney 2000) conducted with a counterflow slot-jet apparatus demonstrate a large variety of non-planar flame structures, such as travelling waves propagating along strips of the flame, stationary and moving single 'flame tubes', and structures resemble chains of the 'flame tubes'. It would be interesting to explain the phenomena of travelling waves by a linear stability analysis extended to the two-dimensional case. Mathematically, the development of small spatial perturbations with non-zero imaginary and positive real parts of growth rate may result in the formation of travelling waves or more complex pulsating spatial modes of the stretched flame front.

5. Numerical simulation

In the direct simulation of Ju *et al.* (2000), although the dependence of the instability on stretch rate was demonstrated for CH_4–air flames, the dependence of the instability on the equivalence ratio was not examined because of computational limitations. In order to prove the validity the present analysis, we need to demonstrate numerically that the near-limit pulsating stability is also bounded to the equivalence interval (the horizontal boundary of instability in figure 10). We again employ axisymmetric counterflow premixed flames with a CH_4–air mixture, together with C1 chemical kinetics and optically thin radiation model. Details and justification of these models can be found in our previous work (Ju *et al.* 1997, 2000). The unburned temperature

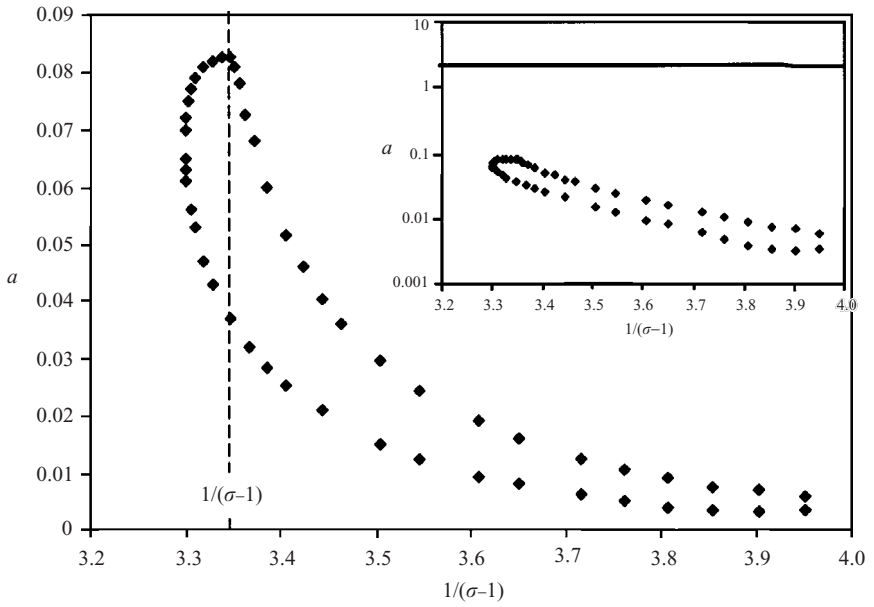

FIGURE 10. The diagram of flame instability plotted as the instability onset velocity gradients a as a function of the reduced flame temperature $1/(\sigma - 1)$ for $Le = 0.9$ and $n = 0$. The region of pulsating instability of stretched flames lies inside the isola. The vertical dashed line corresponds to the lean flammability limits of the unstretched planar propagating flame. In the inset, the thick line denotes the stretch extinction limit of the stretched flame.

of the mixture is 300 K and the pressure is 1 atm, which are the same as those used in the analysis. Unsteady solutions were obtained using a point implicit upwind scheme with an adaptive grid. The initial perturbation is 1% of the local temperature difference with the unburned mixture. The second-order Crank–Nicholson method is employed for time marching. The minimum time step is 1 ms. The time evolution of the flame temperature at a constant stretch rate ($4\,s^{-1}$) for different equivalence ratios is plotted in figure 11. It is seen that, at small equivalence ratio (0.43), the initial perturbation decays rapidly and the flame is stable. As the equivalence ratio is increased to 0.48, the flame initially oscillates when subjected to a small perturbation, but this oscillation decays with time. When the equivalence ratio is increased to 0.485, pulsating instability occurs. This oscillation also exists at an equivalence ratio of 0.487, but disappears at an equivalence ratio of 0.50. Although it is difficult for numerical simulation to exactly define the oscillation boundary, figure 11 clearly shows that there is a window of equivalence ratio within which the flame becomes unstable. This result confirms the validity of the analysis in the previous section.

6. Conclusions

Analytical relations of flame bifurcations and a dispersion equation for the stability of sub- and near-limit stretched flames are derived with both symmetrical and asymmetrical perturbations. In contrast to the classical thermal-diffusion pulsating instability, which only occurs at large Lewis numbers, a new kind of radiation-induced pulsating instability is found to exist for stretched flames at Lewis number close to unity. It is shown that radiation-induced instability occurs at moderate stretch rates on the weak flame and near-stagnation flame branches, rather than near the radiation

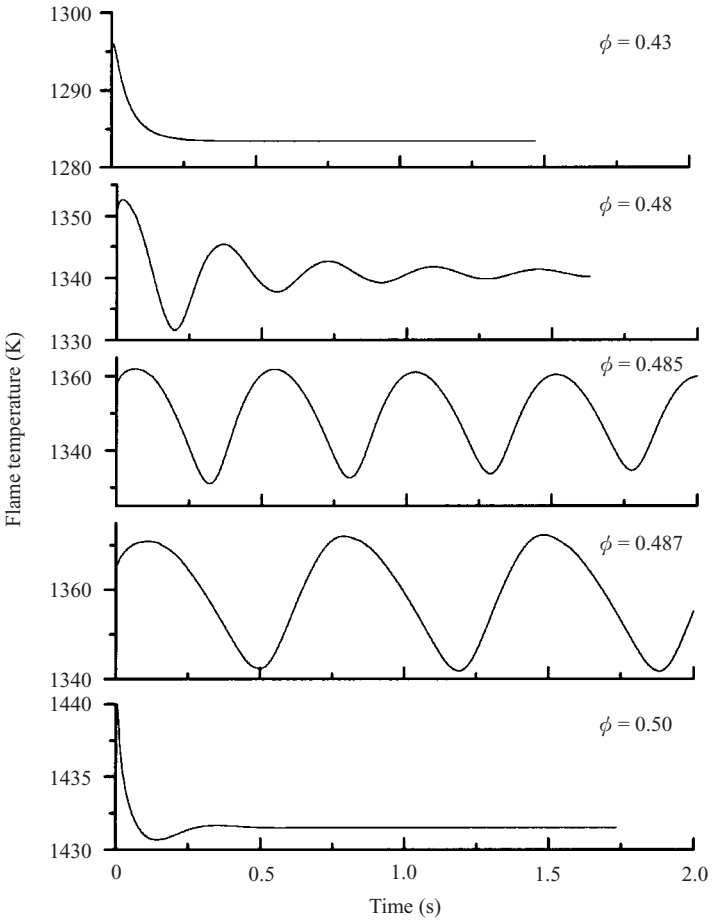

FIGURE 11. Time history of flame temperature for $a = 4\ \mathrm{s}^{-1}$ and $Le = 0.967$ for typical equivalence ratios (detailed numerical simulation).

and stretch extinction limits. A diagram showing the establishment of pulsation instability in terms of the stretch rate and flame temperature is presented. The analytical results agree with numerical simulations, and give a good explanation for the observations of microgravity experiments.

Y. J. would like to thank Professor T. Niioka of Tohoku University and Professor K. Maruta of Akita Prefecture University for many interesting discussions. This work was partly supported by AFOSR under the technical monitoring of Dr J. M. Tishkoff, and the Petroleum Research Fund of the American Society of Chemistry under contract PRF# 39162-AC9.

Appendix

Here we show the general exact solution of (43), various forms of which were employed in the study. The equation can be written in the form

$$-2\varsigma\frac{\mathrm{d}\phi}{\mathrm{d}\varsigma} = \frac{\mathrm{d}^2\phi}{\mathrm{d}\varsigma^2} - 2\Lambda\phi, \tag{A 1}$$

where Λ is a complex number. We restrict ourselves to the case when $\mathrm{Re}(\Lambda) > -1$. Substituting

$$\phi(\varsigma) = \exp(-\varsigma^2)G(\varsigma) \tag{A 2}$$

into (A 1), we have

$$2\varsigma\frac{\mathrm{d}G}{\mathrm{d}\varsigma} = \frac{\mathrm{d}^2G}{\mathrm{d}\varsigma^2} - 2(\Lambda+1)G. \tag{A 3}$$

The general solution of (A 3) can be written as

$$G(\varsigma) = K_1J^-(\varsigma,\Lambda) + K_2J^+(\varsigma,\Lambda), \tag{A 4}$$

$$J^-(\varsigma,\Lambda) = \int_0^\infty \eta^\Lambda \exp\left(-\frac{\eta^2}{4} - \varsigma\eta\right)\mathrm{d}\eta, \tag{A 5}$$

$$J^+(\varsigma,\Lambda) = \int_0^\infty \eta^\Lambda \exp\left(-\frac{\eta^2}{4} + \varsigma\eta\right)\mathrm{d}\eta, \tag{A 6}$$

where K_1, K_2 are arbitrary constants. As one can see from (A 5) and (A 6), the restriction of $\mathrm{Re}(\Omega) > -1$ is necessary for the integrals to converge near zero.

The proof of the above solution is simple. We only demonstrate the validity for a special case of $K_2 = 1$ and $K_1 = 0$; the reader can easily extend it to the general case of arbitrary K_1 and K_2. Substituting (A 6) into the left-hand side of (A 3) and integrating by parts, one obtains

$$\begin{aligned} 2\varsigma\frac{\mathrm{d}G}{\mathrm{d}\varsigma} &= 2\int_0^\infty \varsigma\eta^{\Lambda+1}\exp\left(\varsigma\eta - \frac{\eta^2}{4}\right)\mathrm{d}\eta = \underline{2\int_0^\infty \frac{\mathrm{d}}{\mathrm{d}\eta}\left(\eta^{\Lambda+1}\exp\left(\varsigma\eta - \frac{\eta^2}{4}\right)\right)\mathrm{d}\eta} \\ &\quad -2\int_0^\infty \exp(\varsigma\eta)\frac{\mathrm{d}}{\mathrm{d}\eta}\left(\eta^{\Lambda+1}\exp\left(-\frac{\eta^2}{4}\right)\right)\mathrm{d}\eta \\ &= -2(\Lambda+1)G + \int_0^\infty \eta^{\Lambda+2}\exp\left(\varsigma\eta - \frac{\eta^2}{4}\right)\mathrm{d}\eta \end{aligned} \tag{A 7}$$

The underlined integral in (A 7) becomes zero under the condition of $\mathrm{Re}(\Lambda) > -1$. The right-hand side of (A 3) is given by

$$\frac{\mathrm{d}^2G}{\mathrm{d}\varsigma^2} - 2(\Lambda+1)G = -2(\Lambda+1)G + \int_0^\infty \eta^{\Lambda+2}\exp\left(\varsigma\eta - \frac{\eta^2}{4}\right)\mathrm{d}\eta. \tag{A 8}$$

A comparison between the right-hand sides of (A 7) and (A 8) proves that G is the solution of (A 3). In view of (A 2), the general solution of (A 1) may be written as

$$\phi(\varsigma,\Lambda) = K_1I^-(\varsigma,\Lambda) + K_2I^+(\varsigma,\Lambda), \tag{A 9}$$

where

$$I^-(\varsigma,\Lambda) = \exp(-\varsigma^2)J^-(\varsigma,\Lambda), \quad I^+(\varsigma,\Lambda) = \exp(-\varsigma^2)J^+(\varsigma,\Lambda). \tag{A 10}$$

Let us examine the asymptotic behaviour of logarithmic derivatives $A = \mathrm{d}\ln(I^-)/\mathrm{d}\varsigma$, $B_{S,A} = \mathrm{d}\ln(I^+ \pm I^-)/\mathrm{d}\varsigma$ in the case of $\varsigma \gg 1$. As an example, we only show here the estimation of $A(\varsigma,\Lambda)$. The estimation of $B_{S,A}(\varsigma,\Lambda)$ can be obtained in the same way.

Using the identity

$$\Lambda J^-(\varsigma, \Lambda-1) - \frac{1}{2}J^-(\varsigma, \Lambda+1) - \varsigma J^-(\varsigma, \Lambda) = \int_0^\infty \frac{\mathrm{d}}{\mathrm{d}\eta}\left(\eta^\Lambda \exp\left(-\frac{\eta^2}{4} - \varsigma\eta\right)\right)\mathrm{d}\eta = 0 \quad (A\,11)$$

and the formula for the logarithmic derivative of $J^-(\varsigma, \Lambda)$ on ς

$$\Phi(\varsigma, \Lambda) = \frac{\mathrm{d}}{\mathrm{d}\varsigma}\ln J^-(\varsigma, \Lambda) = -\frac{J^-(\varsigma, \Lambda+1)}{J^-(\varsigma, \Lambda)} \quad (A\,12)$$

one can derive the recurrence formula for $\Phi(\varsigma, \Lambda)$ and $\Phi(\varsigma, \Lambda-1)$:

$$\Phi(\varsigma, \Lambda)\Phi(\varsigma, \Lambda-1) - 2\varsigma\Phi(\varsigma, \Lambda-1) - 2\Lambda = 0. \quad (A\,13)$$

In the case of $\Lambda \gg 1$ and $\varsigma \gg 1$, the function $\Phi(\varsigma, \Lambda-1)$ is close to $\Phi(\varsigma, \Lambda)$ so (A 13) may be rewritten as a quadratic equation for the function $\Phi(\varsigma, \Lambda)$:

$$\Phi(\varsigma, \Lambda)^2 - 2\varsigma\Phi(\varsigma, \Lambda-1) - 2\Lambda = 0. \quad (A\,14)$$

According to (A 12), $\Phi(\varsigma, \Lambda)$ is a negative function. This condition can be applied to the solutions of (A 14) and yields the asymptotic formula for $\Phi(\varsigma, \Lambda)$:

$$\Phi(\varsigma, \Lambda) = \varsigma - \sqrt{\varsigma^2 + 2\Lambda}. \quad (A\,15)$$

By knowing $\Phi(\varsigma, \Lambda)$, one can easily obtain the asymptotic formula for $A(\varsigma, \Lambda)$:

$$A(\varsigma, \Lambda) = \frac{\mathrm{d}}{\mathrm{d}\varsigma}\ln I^-(\varsigma, \Lambda) = -2\varsigma + \frac{\mathrm{d}}{\mathrm{d}\varsigma}\ln J^-(\varsigma, \Lambda) = -2\varsigma + \Phi(\varsigma, \Lambda) = -\varsigma - \sqrt{\varsigma^2 + 2\Lambda}. \quad (A\,16)$$

In the same manner, we can derive the asymptotic formula for $B_{A,S}(\varsigma, \Lambda)$ as

$$B_{S,A}(\varsigma, \Lambda) \cong \frac{\mathrm{d}}{\mathrm{d}\varsigma}\ln I^+(\varsigma, \Lambda) = -\varsigma + \sqrt{\varsigma^2 + 2\Lambda}. \quad (A\,17)$$

In view of (A 9), (A 16) and (A 17), the second solution of (A 9) with constant K_2 approaches infinity at infinitely large ς, whereas the first solution with constant K_1 vanishes with increasing ς.

The selection of the constants K_1 and K_2 depends on the boundary conditions. To satisfy the boundary condition $\mathrm{d}\phi/\mathrm{d}\zeta = 0$ as $\varsigma = 0$, we set $K_1 = K_2$. Solution of (A 9) has the form (see (25)),

$$\phi(\varsigma, \Lambda) = I^-(\varsigma, \Lambda) + I^+(\varsigma, \Lambda) = 2\exp(-\varsigma^2)\int_0^\infty \eta^\Lambda \cosh(\varsigma\eta)\exp\left(-\frac{\eta^2}{4}\right)\mathrm{d}\eta. \quad (A\,18)$$

In the case of $\phi(\varsigma) \to 0$ as $\varsigma \to \infty$, the solution with constant K_2 should be discarded and the remaining term leads to (24) and (42).

REFERENCES

Buckmaster, J. D. 1979 *The Seventeenth Symp. (Intl) on Combustion*, pp. 835–842. The Combustion Inst.

Buckmaster, J. D. 1997 The effects of radiation on stretched flames. *Combust. Theory Modell.* **1**, 1–11.

Buckmaster, J. D., Joulin, G. & Ronney, P. D. 1991 The structure and stability of nonadiabatic flame balls. *Combust. Flame* **84**, 411–422.

Buckmaster, J. D. & Ludford, G. S. 1983 Lectures on Mathematical Combustion CBMS-NSF Regional Conference Series in Applied Mathematics No. 43 SIAM.

Christiansen, E. W., Sung, C. J. & Law, C. K. 1998 Pulsating instability in near-limit propagation of rich hydrogen/air flames. *Proc. Combust. Inst.* **27**, 555–561.

He, L. & Clavin, P. 1993 Premixed hydrogen-oxygen flames. 1. Flame structure near the flammability limits. *Combust. Flame* **93**, 408–420.

Joulin, G. & Clavin, P. 1979 Linear stability analysis of nonadiabatic flames: diffusional–thermal model. *Combust. Flame* **35**, 139–153.

Ju, Y., Guo, H., Liu, F. & Maruta, K. 1999 Effects of the Lewis number and radiative heat loss on the bifurcation and extinction of CH_4/O_2-N_2-He flames. *J. Fluid Mech.* **379**, 165–190.

Ju, Y., Guo, H., Maruta, K. & Liu, F. 1997 On the extinction limit and flammability limit of non-adiabatic stretched methane-air premixed flames. *J. Fluid Mech.* **342**, 315–334.

Ju, Y., Guo, H., Maruta, K. & Niioka, T. 1998 Flame bifurcations and flammable regions of radiative counterflow premixed flames with general Lewis numbers. *Combust. Flame* **113**, 603–614.

Ju, Y., Law, C. K., Maruta, K. & Niioka T. 2000 Radiation induced instability of stretched premixed flames. *Proc. Combust. Inst.* **28**, 1891–1900.

Kailasanath, K., Ganguly, K. & Patnaik, G. 1993 Detailed multidimensional simulations of the structure and dynamics of flames. *Prog. Astro. Aeron.* **151**, 247–262, AIAA, Washington DC.

Kaiser, C., Liu, J.-B. & Ronney, P. D. 2000 Diffusive-thermal instability of counterflow flames at low Lewis number. *38th Aerospace Sciences Meeting & Exhibit, 10–13 January 2000, Reno, Nevada.*

Kitano, M., Kobayashi, H. & Otsuka, Y. 1989 A study of cylindrical premixed flames with heat-loss. *Combust. Flame* **76**, 89.

Kortstarts *et al.* 1997. On the stability of stretched flames. *Combust. Theory Modell.* **1**, 143–156.

Law, C. K. 1988 Dynamics of stretched flames. *Twenty-Second Symp. (Intl) on Combustion*, p. 1381. The Combustion Inst.

Maruta, K., Ju, Y., Honda, A. & Niioka, T. 1998 Lewis number effect on extinction characteristics of radiative counterflow CH_4-O_2-N_2-He flames. *Twenty-Seventh Symp. (Intl) on Combustion*, p. 2611. The Combustion Inst.

Maruta, K., Yoshida, M., Ju, Y. & Niioka, T. 1996 Experimental study on methane-air premixed flame extinction at small stretch rates in microgravity. *Proc. Combust. Inst.* **26**, 1283–1289.

Rogg, B. 1982 In *Numerical Methods in Laminar Flame Propagation* (ed. N. Peters & J. Warnatz) pp. 38–48, Vieweg & Sohn.

Sivashinsky, G. I. 1977 Diffusional–thermal theory of cellular flames. *Combust. Sci. Technol.* **15**, 137–146.

Sivashinsky, G. I. & Law C. K. 1982 On the stability of premixed flames in stagnation-point flow. *Combust. Sci. Technol.* **28**, 155–159.